On Low Frequencies emitted by Air Guns at Very Shallow Depths - An Experimental Study

(March 28, 2019)

Running head: **Low Frequencies from Shallow Air Guns**

ABSTRACT

In marine seismic acquisition the enhancement of the amplitude of frequencies below 5 Hz is of special interest since it improves imaging of the subsurface. The frequency content of the air gun, the most commonly used marine seismic source, is mainly controlled by its depth and the volume. While the depth dependency on frequencies above 5 Hz is thoroughly investigated, for frequencies below 5 Hz it is less understood. However, recent results suggest that sources fired very close to the sea surface might enhance these very low frequencies. Therefore, dedicated tank experiments are conducted to investigate the changes of the source signal for very shallow sources in more detail. A small volume air gun is fired at different distances from the water-air interface, including depths for which the air bubble directly bursts into the surrounding air. The variations of the oscillating bubble and surface disturbances, which can cause changes of the reflected signal from the sea surface, are explored to investigate whether an increased frequency signal below 5 Hz can be achieved from very shallow air guns. The results are compared with field measurements of a large volume air gun fired close to the sea surface. The results reveal an increased signal for frequencies below 5 Hz of up to 10 dB and 20 dB for the tank and field experiments, respectively, for

the source depth where the air gun bubble bursts directly into the surrounding air. For large volume air guns an increased low frequency signal might also be achieved for ~~slightly deeper source depths~~ *sources that are slightly deeper than this bursting depth*. From these observations new design considerations in the geometry of air gun arrays in marine seismic acquisition ~~can be~~ *are* suggested.

INTRODUCTION

The enhancement of signal amplitudes of frequencies below 5 Hz is a desirable objective in marine seismic data acquisition as it would have several benefits. The penetration depth of the signal increases and imaging below complex overburden structures such as basalt or salt would be improved if the low frequencies are enhanced. In addition, low frequencies are beneficial for waveform inversion as they reduce the number of local minima in the least-squares misfit function and the chance to converge towards the true velocity is higher (ten Kroode et al., 2013). However, the generation of low frequencies by seismic air guns, which are the most commonly used marine seismic source, is a major issue due to two counteracting effects. These are the interference of the first reflected signal from the sea surface, referred to as the ghost, with the downgoing wavefield, and the oscillating air bubble produced by the air gun (Hegna and Parkes, 2011). Deep towed sources give stronger low frequency amplitudes due to the ghost effect compared to shallow ones. In contrast, the oscillating air bubble generates stronger low frequency amplitudes for shallower source depths. This is due to longer oscillations of the bubble caused by lower hydrostatic pressure. While the bubble time period controls the frequency output approximately between 5 Hz to 15 Hz, depending on the source depth, the impact of the depth on frequencies below 5 Hz is less understood. However, a few studies indicate that shallow sources might be more likely to produce these very low frequencies (Mayne and Quay, 1971; Landrø and Amundsen, 2014; Amundsen et al., 2017).

The behaviour of oscillating bubbles close to interfaces is studied by several authors for different sizes of air bubbles as mentioned in the following. The differences between air bubbles generated by sparks and explosives close to a solid and free surface is investigated by

Hung and Hwangfu (2010) using high speed photography and pressure gauges. In a similar experimental set up Cui et al. (2016) study the behaviour of underwater explosions in the vicinity of one and two different boundaries, e.g. the free surface and a solid plate with a circular hole. The acoustic signal of small bubbles in the vicinity of interfaces generated by a discharge between two electrodes is discussed by Krieger and Chahine (2005). A numerical model for bubble oscillations close to a plane free surface is demonstrated by Oguz and Prosperetti (1990). An experimental study using a small scale air gun with a volume of 0.88 in^3 (14.5 cm^3) is presented by de Graaf et al. (2014). They investigate the bubble oscillation period and pressure field for different distances to a steel plate and free surface. The variation of the bubble period from an air gun close to the free surface is also discussed by Haavik and Landrø (2016). The interaction of air bubbles in a clustered air gun array, when the sources are close to each other, is studied by Strandenes and Vaage (1992) and Barker and Landrø (2012). The general conclusion of all these studies is that the bubble period increases in the vicinity of a solid boundary. Close to a free surface, alternatively, the bubble period increases until a critical depth where it then decreases.

~~The ghost reflection depends on the water-air interface and when a seismic source is fired at very shallow depths the acoustic pressure that strikes the surface can be large. This could lead to disturbances of the water surface. The accompanying energy loss could lead to a reduced ghost reflection.~~ *The ghost reflection magnitude depends on the water-air interface and the acoustic pressure that strikes the surface from a shallow marine seismic source. A large pressure impulse that is emitted immediately when an air gun is fired can cause variations of the water-air interface.* In seismic acquisition this effect is referred to as the shot effect (Loveridge, 1984, 1985; Parkes and Hatton, 1986). The effect of pressure pulses on a free surface leading to disturbances is also discussed by Temperley and Trevena

(1979). The estimated pressure amplitude needed to break the surface tension and disturb the surface varies for different studies between values of less than one bar to values over 100 bar (Weston, 1960; Nyborg et al., 1972). *Surface disturbances are also caused by the interaction of the oscillating bubble and its radiated pressure with the water-air interface if the bubble is in close vicinity to the free surface.* In addition to the disturbance of the interface, cavitation below the interface can occur caused by the negative reflected pressure pulse (Wentzell et al., 1969). This could also lead to energy losses from the ghost reflection. Another interesting effect that changes the interface shape are Faraday waves (Faraday, 1831). These surface waves can be generated at fluid-fluid interfaces by a periodic vertical motion within one of the fluids which in case of the air gun is caused by the oscillating bubble. Several experimental (Douady and Fauve, 1988; Douady, 1990) and numerical (Périnet et al., 2009, 2012) studies demonstrate the surface wave patterns generated due to harmonic motions in the fluid.

A few more studies should be mentioned that discuss different ways to enhance the low frequency output in marine seismic acquisition. Dellinger et al. (2016) present a vibrator-type source, called Wolfspar, that is designed to create specific ultra-low frequencies needed for the computation of velocity models in full waveform inversion (FWI). A marine dipole source is illustrated by Meier et al. (2015) which would change the ghost notches and hence would amplify the low frequency amplitudes. Ronen and Chelminski (2018) present a new pneumatic source, called the Tuned Pulse Source (TPS), that can use much larger volumes and lower operating pressures compared to conventional airguns. They propose that this source enhances the low frequency signal while reducing the high frequency content which can be harmful for marine life. In addition, using the signal apparition approach in simultaneous source acquisition (Robertsson et al., 2016) could produce signals with

more low frequencies and less high frequencies compared to conventional seismic source acquisition.

We investigate the effects on the air gun signal for sources fired very close to the sea surface in more detail by performing experiments in a water tank and compare those to field measurements (Amundsen et al., 2017). The variations of the bubble period and ghost effect are discussed for sources fired at these shallow depths. In the tank experiment a small volume air gun is fired at different depths including the point where the bubble bursts directly into the surrounding air, breaks the water surface and hence no oscillations occur in water. A test with dynamite charges fired close to the water surface and hence removing the oscillating bubble is presented by Lay (1945). The surface disturbance caused by the acoustic pressure striking the water-air interface is also investigated further depending on the source depth. The results should reveal how valuable very shallow air guns could be for an enhanced low frequency signal below 5 Hz in marine acquisition and which depths might be optimal to achieve these increased low frequency signals.

THEORY

The two main effects that are described in the following are the change of the bubble time period in the vicinity of the free surface and the impact of a reduced ghost reflection on the frequency spectrum. The mechanisms that could be responsible for a decreased ghost reflection are described. For the variation of the bubble time period we follow the explanation given by Haavik and Landrø (2016).

The first description of an oscillating bubble in an inviscid, incompressible and infinite medium is given by Rayleigh (1917) that neglects the effect of the free surface on the bubble.

The maximum bubble radius can be estimated using the assumption of adiabatic expansion (Willis, 1941). This leads to the Rayleigh-Willis equation which is commonly used in seismic acquisition to estimate the bubble time period as (Rayleigh, 1917; Willis, 1941)

$$T_{\mathrm{RW}} = C\ \frac{P_f^{1/3} V_g^{1/3}}{p_h^{5/6}} \tag{1}$$

where P_f is the firing pressure and V_g the volume of the air gun. The constant C is specific for the design of the gun and p_h is the hydrostatic pressure. The impact of an interface such as the free surface was described first by Herring (1941) which corrects the Rayleigh-Willis equation leading to

$$T_{\mathrm{He}} = T_{\mathrm{RW}}\Big(1 + r\frac{R_a}{4z_s}\Big) \tag{2}$$

where R_a is the average bubble radius within one period and z_s is the distance from the interface to center of the bubble. In case of a free surface the reflection coefficient is r = -1 while for a rigid boundary $r = 1$. Similar to this, Haavik and Landrø (2016) derive an expression to correct the bubble time period for the case where the bubble is close to an interface. They suggest to compute the bubble time period as

$$T_{\mathrm{HL}} = T_{\mathrm{RW}}\frac{1}{2}\sqrt{A(\kappa, r)} \tag{3}$$

where

$$A(\kappa, r) = \frac{4\kappa + 4r - r^2 \ln(\frac{\kappa-1}{\kappa+1})}{\kappa} + \frac{2r^2}{1-\kappa^2}\ , \kappa \geq 4. \tag{4}$$

The parameter κ describes the ratio of the distance to the interface and the equilibrium bubble radius R_{eq} as $\kappa = 2z_s/R_{eq}$. The radius R_{eq} is the bubble size when the pressure inside and outside the bubble is equal. The change of the bubble time period as a function of source depth z_s for different gun sizes is illustrated in Figure 1. We notice that the bubble time period increases for decreasing source depths z_s until a turning point (Figure 1, circles).

For source depths shallower than this turning point the bubble period decreases again and hence the low frequency content is not increased anymore due to the oscillating bubble. An interesting observation is that the ratio z_s/R_{max} between source depth and maximum bubble radius, assuming an oscillating bubble after Rayleigh (1917) at the turning point decreases for increasing air gun sizes as z_s/R_{max} = 2.34 (100 in^3), 1.86 (500 in^3) and 1.67 (1200 in^3). The maximum bubble radius R_{max} can be estimated as (Rayleigh, 1917; Willis, 1941)

$$R_{max} = \frac{T_b}{1.83\sqrt{\rho/p_h}} \tag{5}$$

where ρ is the density of water, T_b the bubble time period and 1.83 is an exact number derived from gamma functions by Rayleigh (1917).

[Figure 1 about here.]

For a simple illustration of the ghost effect on the frequency content we assume a point source that emits a spike function which excludes the impact of the oscillating bubble *and the peak width of an air gun signal*. The frequency spectrum of the sampled time signal $s(n)$ can be computed using the discrete Fourier transform as (Ikelle and Amundsen, 2005)

$$S(k) = \sum_{n=0}^{N-1} s(n)\ e^{-i2\pi nk/N} \tag{6}$$

$$s(n) = \frac{1}{N}\sum_{k=0}^{N-1} S(k)\ e^{i2\pi nk/N} \tag{7}$$

where N is the number of samples. The values of $s(n)$ and $S(k)$ are sampled at times $t_n = t_{\text{start}} + n\Delta t$ and frequencies $f_k = k\Delta f$ with $n = k = 0, 1, ..., N-1$. If we assume a perfect reflection at the water-air interface, with a reflection coefficient of r = -1, the signal and frequency spectrum can be computed for different source depths z_s as illustrated in Figure 2 (dashed line). The time delay t_d of the ghost reflection corresponds to $t_d = 2z_s/c$,

where $c = 1500$ m/s is the sound velocity in water. This is valid for the normal incidence case and in the far-field where the source-receiver distance is much larger than the source-interface distance and hence amplitude differences between the direct spike and ghost spike due to the distance $2z_s$ can be neglected.

[Figure 2 about here.]

If we assume that the ghost amplitude is reduced due to energy losses at the surface related to the acoustic pressure that strikes the surface, we could assume a smaller ghost amplitude for shallower sources (Loveridge, 1984, 1985). For the reduced ghost shown in Figure 2 (solid line) we use the empirical relation presented by Hatton (2007) which leads to variations of the reflection coefficient r as

$$r = 1.3\Big(\frac{p_p}{z_s}\Big)^{1/5} - 1.7 \tag{8}$$

where p_p is the zero to peak pressure in bar-m and r is constrained in the range -1 to -0.3. For the example in Figure 2 a peak pressure of $p_p = 1$ bar-m is assumed for all source depths. It should be noted that the reflection coefficient might only vary temporarily when the acoustic pressure exceeds a critical value at the surface. The spectra in Figure 2 can also be described by the ghost function, assuming vertically travelling plane waves, as (Amundsen and Zhou, 2013)

$$|G| = |1 + r\ e^{(2i\frac{2\pi f z_s}{c})}|. \tag{9}$$

We notice in Figure 2 that a reduced ghost reflection fills up the notches related to the source depth, e.g. at 187.5 Hz and 250 Hz for a source depth of 3 m and 4 m, respectively. This could be of special interest for low frequencies. For the shallowest source at 2 m the reduced ghost amplitude leads to a higher amplitude content of 10 - 25 dB between frequencies of 1 - 5 Hz compared to the deeper sources. As the reduced reflection coefficient depends on the

distance between the source and water-air interface, the effect is less pronounced at larger take-off angles. If we replace z_s with $z_s/cos(\theta)$ in Equation 8, where θ is the take-off angle, the amplitude enhancement between 1 - 5 Hz for a source depth of $z_s = 2$ m is reduced by 3.9 % at $\theta = 30^o$ compared to the normal incident case. At shallower source depths the difference with take-off angle is less pronounced. For the example in Figure 2 a constant peak pressure of $p_p = 1$ bar-m is assumed for all source depths. That the peak amplitude does not change with source depth is empirically demonstrated by Vaage et al. (1983) for source depths between 5 and 12 m and source volumes between 40 and 580 in^3. Modeling of the source signature, using the damped Kirkwood-Bethe equation (Landrø and Sollie, 1992), does not indicate variations of the peak amplitude for shallower source depths than 5 m. However, the modeling accounts for variations of the hydrostatic pressure and not for non-linear interactions when the bubble breaks the surface. Therefore, it is not certainly known if the peak pressure varies at very shallow source depths.

The potential mechanisms that lead to energy losses at the sea surface and therefore to a reduced ghost reflection could be divided into three parts. The first effect is the interaction of the acoustic pressure with the water-air interface as discussed before and shown in Figure 2 (Loveridge, 1984; Hatton, 2007). Secondly, there is the physical interaction of the source (air bubble) with the interface. If the air gun is so close to the surface that the bubble directly bursts into the air, the surface is highly disturbed and the water-air interface almost vanishes at the point where the bubble breaks. This could cause a strong decrease of the ghost reflection while it should be mentioned that the overall source signal strength is expected to decrease compared to deeper sources. Thirdly, a rough sea surface, caused by wind and weather, impacts the reflected signal as discussed by many authors (Brekhovskikh and Lysanov, 1991; Hovem, 2007; Jensen et al., 2011). However, this mostly effects higher

frequencies in seismic acquisition and hence stronger sea states are expected to reduce the higher ghost notches (Jovanovich et al., 1983) but not the notch at 0 Hz. Therefore, we do not elaborate more on the effect of a rough sea surface.

EXPERIMENTS

For a detailed investigation of very shallow sources we conduct experiments in a water tank where the source is fired almost at the water-air interface. In addition, we investigate data from a field experiment where a large volume air gun is fired in a fjord at different source depths (Amundsen et al., 2017).

Water tank experiments

The experiments are conducted in a water tank with the dimensions shown in Figure 3. The walls of the tank are equipped with 5 cm thick foam mattresses. This damping material leads to an improved signal reception with smaller side reflections indicated by previous tests, although they do not act as perfectly absorbing boundaries. The source is a Mini G. Gun with a chamber volume of 12 in^3 which is fired at different depths during the experiment, ranging from $z_s = 0.8$ m to $z_s = 0.1$ m (Figure 3).

[Figure 3 about here.]

Brüel & Kjær hydrophones of the type 8105 are used as receivers for all experiments in the tank which have a flat frequency response from 0.1 Hz to 100 kHz. An additional hydrophone is located in air, denoted by H_3 (Figure 3), to record the signal transmitted through the water-air interface. The hydrophones of type 8105 have the same sensitivity in water and air for frequencies up to 3 kHz. Next to the hydrophone H_3 camera 1 is placed

to film the water surface while the air gun is fired at different depths. For the same purpose the camera is also placed at a second location denoted as camera 2. The recording rate of the camera is 240 frames per second (fps) which allows to have a photo approximately every 4.2 ms. The video recordings might provide additional information about the impact on the ghost reflection when an air gun is fired very close to the water-air interface.

The experiment is also repeated several times where the hydrophones H_1 and H_2 are placed at different positions and depths in the water tank to investigate how the tank size influences the received signals. It is concluded that the main observations described in this paper are the same for all tests. The percentage of non-repeatability of the air gun shots at each source depth is described by

$$\delta A = \frac{\frac{1}{N}\sum_{n=1}^{N}(A^{rms} - A_n^{rms})}{A^{rms}} \cdot 100 \tag{10}$$

where A_n^{rms} is the root mean square amplitude of a single recorded trace where n indicates the shot number and N the total number of shots at one depth. A^{rms} is the root mean square amplitude of the stacked traces of all shots at one source depth. For an average number of 10 shots at each source depths, which are 300 Hz low-pass filtered, a non-repeatability of $\delta A \leq 5\%$ is found.

Field experiments

We analyze data from a field test conducted in a Norwegian fjord (Amundsen et al., 2017). The water depth at the test site is approximately 390 m and the weather conditions were excellent during the test as the sea was calm. Hence, the noise level at low frequencies was not significant as indicated from ambient noise measurements (Amundsen et al., 2017). A Bolt 1500LL single air gun with a chamber volume of 1200 in^3, which is deployed from an

A5 buoy, is fired at different source depths, z_s, below the sea surface (Figure 4).

[Figure 4 about here.]

The signal is recorded with a Reson hydrophone TC4043 that is located at a constant depth of 80 m nearly vertically below the source. The rope with the hydrophone has a weight attached at the end to hold it straight. The x-coordinate for the receiver position given in Figure 4 is an estimation and might vary slightly. The hydrophone has a flat frequency response between 2 Hz and 80 kHz. The air gun was fired at source depths of z_s = 1.3, 2.3, 3.3, 5.3, 7.3, 10.3, 20.3, 30.3 m. For the shallowest depth of 1.3 m one shot was fired. In addition, one shot is conducted between 1.3 m and 2.3 m. The source depths is not exactly known as the air gun is lowered due to a leakage in the A5 buoy. For all sources at a depth of 2.3 m and deeper at least six shots are fired. A more detailed description of the experiment is given by Amundsen et al. (2017). These data were not originally collected to test the hypothesis of low frequency enhancement from very shallow sources, but provide valuable empirical data for analysis.

RESULTS

The pressure recordings of the tank and field experiment are investigated and compared. In addition, the variation of the oscillating bubble for different source depths and air gun sizes is investigated.

Water tank measurements

The measurements of the 12 in^3 air gun fired with a pressure of 80 bar at four different source depths are shown in Figure 5. The signal is corrected for geometrical spreading with $1/r$

where r is the source-receiver distance. The main peak of the air gun signature is reduced with decreasing source depth and the same can be observed for the peak of the oscillating bubble. For a source depth of 0.15 m only one bubble oscillation can be seen around 0.05 s. The signature of the shallowest source depths of 0.1 m does not have any bubble oscillation, indicating that the pressurized air from the gun directly bursts into the air. The maximum bubble radius for the different source depths could be roughly estimated using Equation 5 and the measured bubble period from the recordings. This reveals a maximum bubble radius for the different source depths of $R_{max}(0.15\text{ m}) = 0.19$ m, $R_{max}(0.3\text{ m}) = 0.23$ m and $R_{max}(0.5\text{ m}) = 0.25$ m. It should be noticed that the bubble radius is larger than the source depth for the the source at 0.15 m for this simple approximation. That the bubble vanishes for the shallowest source is visible in the frequency spectra (Figure 5, middle). While the source at 0.15 m still has energy at the first bubble peak at 23 Hz, peaks at higher frequencies related to a 2nd or 3rd bubble oscillation are not present. In addition, the first notches around 36 Hz and 58 Hz related to the bubble oscillation are not present for the source at 0.15 m compared to the deeper sources. The spectrum for the shallowest source at 0.1 m is nearly flat and has no energy related to the oscillating bubble. A close up on the low frequency end of the spectrum (Figure 5, bottom) illustrates that the energy drops for decreasing source depth except for the shallowest source at 0.1 m. For the shallowest source depth a higher amplitude low frequency signal between 2 Hz and 5 Hz can be observed with a gain up to 10 dB compared to the deeper sources. It should be mentioned that frequencies below 0.5 Hz are filtered out. Figure 6 shows photos taken when the air gun is fired at a source depth of 0.15 m in the water tank.

[Figure 5 about here.]

[Figure 6 about here.]

A detailed investigation on the variation of the bubble period is shown in Figure 7. The left end of the x-axis is terminated at the depth where $z_s \approx R_{max}$. The measured bubble time period for source depths between 0.2 m and 0.8 m is compared to the modeled period following Equations 1, 2 and 3. The Rayleigh-Willis equation (T_{RW}) has the largest deviation as it assumes an infinite medium. The measured data matches best with Equation 3 given by Haavik and Landrø (2016). However, the difference to Equation 2 from Herring (1941) is small. In general, a decreasing bubble period with decreasing source depths can be observed for the measured data. Therefore, the highest peak in the spectrum, around 25 Hz, produced by the oscillating bubble is shifted towards higher frequencies as indicated in Figure 5 (middle) for the 12 in^3 used in the tank. The turning point where the bubble period starts to decrease with decreasing source depth is at $z_s \approx 3.2\ R_{max}$.

[Figure 7 about here.]

Field measurements

The measurements of the 1200 in^3 air gun fired with a pressure of 137 bar at four different source depths are shown in Figure 8. We estimate the source depth of the second shallowest source to be at 1.8 m from a notchlike event around 400 Hz and from the bubble period indicated by the peak around 5 Hz in the frequency spectrum (Figure 8, bottom). However, as it is not exactly known and only one shot is conducted we denote the depth in quotation marks. The main peak amplitude of the air gun signature is reduced with decreasing source depth from 7.4 bar at $z_s = 3.3$ m to 6 bar at $z_s = 1.3$ m. The signal is corrected for geometrical spreading using $1/r$ to get the amplitude at 1 m distance from the source. A

large amplitude difference can be observed for the bubble peak which is also reduced for decreasing source depths.

[Figure 8 about here.]

For the shallowest source at 1.3 m no oscillating bubble can be observed in the time recordings, again indicating that the pressurized air from the gun directly burst into the air. For the source at "1.8" m at least one bubble oscillation is observed in the frequency spectrum (Figure 8, bottom) where the notch around 8 Hz is still pronounced compared to the shallowest depth, although the bubble oscillation is difficult to identify on the pressure recordings (Figure 8, top). The maximum bubble radius for the different source depths is estimated using Equation 5 and the measured bubble period from the recordings. This reveals a maximum bubble radius for the different source depths of $R_{max}(1.8\text{ m}) = 1.19$ m, $R_{max}(2.3\text{ m}) = 1.22$ m and $R_{max}(3.3\text{ m}) = 1.23$ m. While the source at 2.3 m still has sufficient energy from the oscillating bubble visible at frequencies below 50 Hz, the spectrum for the shallowest source at 1.3 m is nearly flat according to the vanishing bubble oscillation (Figure 8, middle). In addition, the ghost notch for the source at 3.3 m is visible around 200 Hz. A close up on the low frequency end of the spectrum (Figure 8, bottom) illustrates that the energy drops for decreasing source depths related to the reduced energy of the bubble oscillation. For the shallowest source at 1.3 m a higher low frequency signal between 0.5 Hz and 2 Hz can be observed with a gain up to 20 dB compared to the deeper sources. It should be mentioned that frequencies below 0.5 Hz are filtered out. In addition, the flat frequency response of the hydrophone used for the field test is between 2 Hz and 80 kHz and hence care must be taken when investigating absolute values at these low frequencies. However, the relative variations of the amplitudes with changing source depth are meaningful and

an enhanced low frequency content can be observed similar to the experiments in the tank (Figure 5).

A detailed investigation on the variation of the bubble period is shown in Figure 9.

[Figure 9 about here.]

The measured bubble time period for source depths between 1.8 m and 30.3 m is compared to the theory. The best fit between the measured and modelled bubble time period for this data is given by Herring (1941). However, the difference between T_{He} and T_{HL} for the range of measured source depths is very small. In general, an increasing bubble time period T_b with decreasing source depths can be observed for the measured data which should lead to an enhanced low frequency signal produced by the oscillating bubble, assuming that the amplitude would be constant. It should be noted that the bubble period increases for source depths as shallow as $z_s \approx 1.6\ R_{max}$. Therefore, the turning point where the bubble period starts to decrease with decreasing source depth is shallower than for the small 12 in^3 air gun (Figure 7) relative to the maximum bubble radius.

Energy vs. Depth

The energy variation of the acoustic signal with source depth for the tank and field experiments is investigated for the measurements in water and air. The acoustic energy of the air gun for different source depths is estimated from the frequency spectra as

$$E = \int_{f_l}^{f_u} |S(f)|^2 df \tag{11}$$

where $S(f)$ is the Fourier transform of the recorded, stacked traces for each source depth z_s and f_l, f_u are the lower and upper frequency limit used for the integration. The stacked

traces are corrected for geometrical spreading with $1/r$ where r is the source receiver distance. The results in Figure 10 illustrate the normalized energy variations with source depths in the frequency band from 1 Hz (f_l) to 400 Hz (f_u). The energy in air, measured at H_3 (Figure 3), increases with decreasing source depth (Figure 10, top). In contrast to that, the energy in water from the tank experiment decreases with decreasing source depth. In general, the comparison between the energy in air and water illustrates that the loss in water anticorrelates well with the increase in air for the measurements in the tank, although the absolute energy difference between water and air is large. The field measurements (Figure 10, bottom) have the same trend *in the water column* as the results in the tank with a decrease in energy for shallower sources. Despite the increased energy for frequencies below 5 Hz and 2 Hz for the shallowest sources in Figure 5 (bottom) and Figure 8 (bottom), respectively, the acoustic energy can be expected to be smaller for very shallow sources compared to deeper ones. The main reason is the reduced energy of the oscillating air bubble for decreasing source depths. For air gun arrays that are tuned on the main peak and a reduced bubble oscillation, the decrease of acoustic energy with source depth might be less pronounced.

[Figure 10 about here.]

Surface disturbance

We estimate a critical pressure that is required to ~~visible~~ *visibly* disturb the water-air interface in the tank experiments from video recordings and the acoustic measurements. We assume that the pressure radiates spherically from the source as shown in Figure 11(a). The video recordings are used to determine the radius d of the disturbed surface, estimated

from marks along the rope in Figure 11(b). The critical distance r_c is calculated from the known source depth as $r_c = \sqrt{d^2 + z_s^2}$. For an estimation of the critical pressure we use measurements of 15 shots recorded at the receivers H_1 and H_2 for source depths of z_s = 0.2, 0.3, 0.4, 0.5, 0.6 m. The critical pressure is computed as

$$p_c = \frac{1}{2} \sum_{i=1}^{2} \frac{1}{N} \sum_{n=1}^{N} \max(p_{i,n}) \left(\frac{r_i}{r_c} \right)^m \tag{12}$$

where $\max(p_{i,n})$ is the maximum measured pressure of shot number n at the receiver number i, where i = 1,2 and N is the number of recordings. The source-receiver distance is denoted by r_i as shown in Figure 11(a). The factor m = 1,2 accounts for a linear and quadratic spreading correction, respectively. Assuming a linear spreading correction for the amplitudes an average critical pressure from both hydrophones of $p_c = 1.11 \pm 0.20$ bar can be estimated for unfiltered pressure recordings. For the quadratic spreading correction, the critical pressure is $p_c = 1.09 \pm 0.16$ bar. The small variation between both results can be explained by small differences of the distances r_c and r_i.

[Figure 11 about here.]

DISCUSSION

The effects and mechanisms that have an impact on the low frequency signal from very shallow air guns are discussed in light of these results. These effects and mechanisms are the changing bubble time period with distance to the interface and the vanishing bubble oscillation when the bubble breaks the surface. In addition, as the source depth is decreased the water surface is disturbed by the acoustic pressure striking the surface and the expanding bubble. All these effects acting on the water-air interface can be expected to cause changes to the ghost reflection. We also discuss recommended depths and air gun volumes for a

potential enhancement of frequencies below 5 Hz.

A possible mechanism for energy loss of the ghost reflection is the disturbance of the water surface caused by the acoustic pressure striking the interface as discussed before (Figure 11). This is similar to the explanation by Weston (1960) and Loveridge (1985) that a critical pressure p_c is required to break the surface tension at the sea surface. Although the estimated critical pressure, $p_c \approx 1.1$ bar, is a rough estimation and the tank size could influence the measurements, the results agree with observations made from field tests. In a fjord test with a 600 in^3 air gun (Haavik and Landrø, 2016) the shot effect can be observed from video recordings down to a source depth of 5 m. A zero-to-peak pressure of approximately 5 bar-m is measured for these tests, which would result in a pressure of 1.25 bar striking the water surface for a source depth of 5 m when a linear spreading correction is assumed. It should be noted that the shot effect *and surface disturbances* could lead to an increased low frequency signal for very shallow sources as indicated in Figure 2, especially for large volume air guns with a high zero-to-peak pressure amplitude. *The enhancement of amplitudes at low frequencies depends on the magnitude of the initial pulse and the ratio of this peak amplitude to its corresponding ghost amplitude. The measured peak amplitudes (Figure 5 and 8) are reduced with decreasing source depths in contrast to the ghost model (Figure 2). This is most likely caused by the overlap of the main impulse with its ghost reflection as the air gun signal has a certain peak width compared to the spike model. Therefore, the enhancement of amplitudes at low frequencies is also controlled by the peak width of the main impulse.*

Another effect is the bubble time period T_b and the amplitude of the bubble signal and its impact on the low frequencies with a peak at the bubble frequency $f_b = 1/T_b$. Although it is commonly assumed that the bubble enhances the low frequency signal due

to an increasing period with decreasing source depths, at a specific depth close the surface the bubble period decreases again, indicated as the turning point in Figure 1 (circles). This turning point depends on the gun size and for larger gun volumes the sources can be towed shallower relative to its maximum bubble radius (z_s/R_{max}) before this point is reached. This hypothesis is supported by the measurements as the turning point for the 12 in^3 air gun is at $z_s/R_{max} \approx 3.2$ (Figure 7) and for the 1200 in^3 air gun it is at $z_s/R_{max} \approx 1.6$ (Figure 9).

In the tank experiment only near-field signatures are measured and it could be argued that the enhanced amplitudes at low frequencies vanish in the far-field due to the ghost effect. The far-field ghost is not added to the measured data as the effect of the reduced sea surface reflection caused by the surface disturbance is difficult to quantify. However, the similarities for the signal of the shallowest source in the tank, at 0.1 m (Figure 5), and in the field, at 1.3 m (Figure 8), at low frequencies indicate that the ghost is strongly reduced. Therefore, an enhanced low frequency signal in the far-field could still be expected. It should be noted that improvements of the received signal depend not solely on the enhanced source signal but mainly on the signal-to-noise ratio. For our experiments the signal is way above the noise level as the measurements are not too far from the source. The background noise could vary significantly between seismic surveys, but general noise levels for ocean bottom seismometers and marine streamers are demonstrated by Dahm et al. (2006), Smith (1999) and Elboth et al. (2009).

As an attempt to summarize the impact of the source depth on the low frequency part of the signal, characteristic depths are defined for different source volumes (Figure 12, left). The data points in Figure 12 are from the experiments and a second fjord test (Haavik and Landrø, 2016). The impact on the low frequency signal (< 5 Hz) is illustrated by δf_{low}

(Figure 12, right) that schematically demonstrates whether the low frequency part could be enhanced or reduced relative to deep towed sources, where no interaction between the source and water-air interface occurs. In addition, the contributions of the bubble period and ghost effect to the generation of the low frequency signal are schematically shown. For depths shallower than zone V no measurements are available and hence the area is left blank (Figure 12, right). The different zones in Figure 12 are explained in the following.

[Figure 12 about here.]

I No relevant interactions between the source and the water-air interface are expected within this range that have an impact on the source signal. The bubble and ghost effect counteract each other at the low frequency end (Figure 12, right).

II $p_s = p_c$: this depths indicates when the emitted acoustic pressure at the surface p_s equals the critical pressure p_c which was estimated in the experiments and is illustrated in Figure 11. Therefore, the surface could be noticeably disturbed by the shot effect for sources that are fired shallower. Although it is difficult to quantify *the magnitude of* this effect it could reduce the ghost impact as indicated in Figure 2 which could lead to increased amplitudes at low frequencies (Figure 12, right). The source depths for $p_s = p_c$ is estimated as $z_s = (p_p/p_c)+1$ m where p_p is the zero-to-peak amplitude in bar-m. The peak amplitude p_p is computed with the damped Kirkwood-Bethe model (Landrø and Sollie, 1992) that is scaled to measured data of a 12 in^3, 600 in^3 and 1200 in^3 airgun.

III $z_s < 4\ R_{max}$: for all depths smaller than $4 \cdot R_{max}$ the bubble is expected to interact with the sea surface (Chahine, 1977) which leads to a smaller increase of the bubble period than predicted by the Rayleigh-Willis equation (Figure 7 and 9). Therefore, the

increase of low frequencies is lower than assumed, which would counteract the effect described in point II. For large gun volumes the shot effect could be strong within this range while the bubble period still increases (Figure 9). This could be an explanation for the increased low frequencies between 0.5 Hz and 2 Hz for the 1200 in^3 air gun fired at a depth of 3.3 m (Figure 8, bottom). The maximum bubble radius R_{max} is estimated using the damped Kirkwood-Bethe equation (Landrø and Sollie, 1992).

IV T_b decreases: this depth indicates the turning point from which on the bubble period decreases with decreasing source depths (Figure 1, circles) and hence the low frequency enhancement due to the bubble *period* is stopped. This effect is even more pronounced by a reduced bubble amplitude. Measurements within this range could have a reduced low frequency signal compared to zone III (Figure 12, right). *Therefore, zone IV might deviate from a direct relationship where amplitudes at low frequencies are expected to be increased with decreasing source depth.* This hypothesis can be supported by the 12 in^3 air gun fired at 0.15 m (Figure 5) and the 1200 in^3 air gun fired at "1.8" m and at 2.3 m (Figure 8).

V $R_{max} \geq z_s \geq R_{max}/1.5$: within this range it is expected that the bubble breaks the surface. It can be observed from the measurements with the 12 in^3 air gun that the depth might has to be smaller than the maximum radius to break the surface. However, the value of 1.5 is a rough estimation from the observations. Within this range the low frequency signal below 5 Hz is expected to be enhanced the most (Figure 12, right). This could be due to a highly reduced ghost reflection as the surface is strongly altered by the bubble breaking the surface. For even shallower source depths no measurements are available. The lower boundary of this zone might be even shallower as the main

peak of the source signal is emitted way before the maximum bubble radius is reached. However, the energy in water could be highly reduced and more energy goes into air as discussed (Figure 10).

It should be mentioned that this is a simplified and heuristic explanation as the shot effect ~~and~~ *as well as the* nonlinear effects~~,~~ when the bubble breaks the surface~~,~~ are difficult to quantify. In addition, the critical pressure p_c is estimated from experiments with a flat surface and this value could vary when the surface is already disturbed due to weather or waves. Despite all these simplifications the scheme (Figure 12) explains the main effects and observations in the measured data. However, more data is required to adjust and verify the different zones and the sketch could act as a guideline for further field experiments.

To enhance the frequency ~~part~~ *spectrum* below 5 Hz in marine seismic surveys it can be beneficial to place a few sources very shallow as suggested by Amundsen et al. (2017). The depths should be around the range $R_{max} \geq z_s \geq R_{max}/1.5$ as indicated in Figure 12. It is recommended to use large volume air guns due to several reasons. ~~They do not~~ *Large guns do not* lose as much energy from the oscillating bubble as smaller sources when towed that shallow. *Depending on the signal-to-noise ratio, only one or two big air guns (e.g. 1200 in^3) added as a supplement to the conventional array might be sufficient to increase the low frequency signal noticeably. These supplemental guns can be towed at depths around 1 m. It should be mentioned that the towing of air guns as shallow as 1 m or less is a challenging operational task, especially when the sea state is high. However, when this towing issue is solved the addition of a few very shallow sources to a conventional air gun array is very likely to enhance frequencies below 5 Hz. In addition, it seems promising that a 1200 in^3 air gun also enhances the low frequency content for tow depths between 3 m to 4 m (Figure 8), which*

would make towing less complicated. ~~Only one or two big air guns (e.g. 1200 in^3) might be sufficient to increase the low frequency signal noticeable, depending on the signal-to-noise ratio. They can be towed at depths around 1 m and not as shallow as 0.5 m or less which would make the towing even more complicated. In addition, it seems promising that a 1200 in^3 air gun also enhances the low frequency content for depths between 3 m to 4 m (Figure 8). It should be mentioned that the towing of air guns as shallow as 1 m or less is a challenging operational task, especially when the sea state is high. However, when this issue is solved the addition of a few very shallow sources to a conventional air gun array is very likely to enhance frequencies below 5 Hz. The energy related to the oscillating bubble that is lost for very shallow sources needs to be compensated by the conventional part of the array.~~

The generation of low frequencies ($<$ 5 Hz) from very shallow air guns is compared to the alternative sources mentioned in the beginning, namely the Wolfspar (Dellinger et al., 2016) and Tuned Pulse Source (Ronen and Chelminski, 2018). The Wolfspar is taylor-made to generate sweeps between 2-8 Hz or to generate hums at specific frequencies down to 1.35 Hz. ~~and~~ Dellinger et al. (2016) compare measured data of the Wolfspar to recordings of an air gun array. For a single frequency hum at 1.8 Hz the signal from the Wolfspar is 40-45 dB stronger than from a conventional air gun array, while for a sweep between 2-8 Hz the signal amplitude for the Wolfspar is enhanced up to 18 dB below 3.5 Hz compared to the conventional air gun array (Dellinger et al., 2016). If only specific low frequencies are required for velocity model building, ~~than~~ the Wolfspar is superior to the *proposed* shallow tow of air guns. However, this goes in hand with sacrificing a broader bandwidth and higher frequencies. The Tuned Pulse Source generates a longer bubble period by using larger chamber volumes and lower operating pressures than conventional air guns.

The large volumes of the TPS result in a long bubble period and long rise time of the main peak (Ronen and Chelminski, 2018). Modeling predicts that the Tuned Pulse Source could generate stronger signal amplitudes between 15-30 dB for frequencies below 4 Hz compared to air gun arrays with conventional chamber volumes and firing pressures (Ronen and Chelminski, 2018), while the long rise time of the TPS mitigates the high frequency content. *The enhancement of amplitudes for frequencies below 5 Hz from the TPS seems to be comparable to the proposed shallow tow of air guns. However, for higher frequencies (> 5 Hz) the signal from the TPS is expected to be stronger due to the contribution from the oscillating bubble.*

To investigate the effect on the ghost in a field trial in more detail air guns with small bubble oscillations, e.g. GI Guns with two chambers, should be tested, while near- and far-field signals are recorded. The GI gun consists of two chambers, referred to as generator and injector. The injector chamber releases its air with a time delay into the bubble generated by the first chamber and hence the bubble oscillation is reduced. ~~This allows to focus on the main peak and its ghost as the bubble is a strong factor that impacts the signal very close to the sea surface.~~ *This bubble damping concentrates the wavelet energy in the main peak and its ghost rather than the bubble, which is a strong factor that impacts the signal very close to the surface.* This test would continue the work done by Mayne and Quay (1971).

CONCLUSION

An enhanced low frequency signal for frequencies below 5 Hz can be observed in the experiments for sources at a depth where the air gun bubble bursts directly into the air and hence no oscillations occur. For large volume air guns the low frequency signal might be also increased for slightly deeper sources as the high zero-to-peak pressure leads to strong dis-

turbances of the sea surface caused by the acoustic pressure. This could result in a reduced ghost reflection and enhanced low frequency signal as observed in the data. In comparison to small air guns, large volume air guns can be towed at shallower depths relative to their maximum bubble radius before the bubble period starts to decrease in the vicinity of the free surface. Recommended depths are given where guns of different volumes could be placed to achieve an increased signal for frequencies below 5 Hz. In addition, depths are indicated where the oscillating bubble loses most of its energy and where the ghost might start to be reduced. As very shallow air guns, which burst directly into the surrounding air, lose the energy related to the oscillating bubble, a combined source array of a few very shallow air guns and a conventional set up can be a good ~~compromise~~ *combination*. Further field trials are required to verify the results in common marine seismic acquisition surveys and to investigate the feasibility and source signal repeatability of towing air guns as shallow as 1 m, especially during higher sea states.

REFERENCES

Amundsen, L., H. Westerdahl, Å. S. Pederson, M. Thompson, and M. Landrø, 2017, On firing an air gun very shallow: Geophysics, **82**, no. 3, A25–A29.

Amundsen, L., and H. Zhou, 2013, Low-frequency seismic deghosting: Geophysics, **78**, WA15–WA20.

Barker, D., and M. Landrø, 2012, Simple expression for the bubble-time period of two clustered air guns: Geophysics, **77**, A1 – A3.

Brekhovskikh, L. M., and Y. P. Lysanov, 1991, Fundamentals of ocean acoustics: Springer.

Chahine, G. L., 1977, Interaction between an oscillating bubble and a free surface: Journal of Fluid Engineering, **99**, 709 – 176.

Cui, P., A. M. Zhang, and S. P. Wang, 2016, Small-charge underwater explosion bubble experiments under various boundary conditions: Physics of Fluids, **28**, 1 – 24.

Dahm, T., F. Tilmann, and J. P. Morgan, 2006, Seismic broadband ocean-bottom data and noise observed with free-fall stations: Experiences from long-term deployments in the North Atlantic and the Tyrrhenian Sea: Bulletin of the Seismological Society of America, **96**, 647 – 664.

de Graaf, K. L., P. A. Brandner, and I. Penesis, 2014, The pressure field generated by a seismic airgun: Experimental Thermal and Fluid Science, **55**, 239 – 249.

Dellinger, J., A. Ross, D. Meaux, A. Brenders, G. Gesoff, J. T. Etgen, and J. Naranjo, 2016, Wolfspar, an FWI-friendly ultra-low-frequency marine seismic source: 86th Annual International Meeting, SEG, Expanded Abstracts, 4891–4895.

Douady, S., 1990, Experimental study of Faraday instability: Journal of Fluid Mechanics, **221**, 383 – 409.

Douady, S., and S. Fauve, 1988, Pattern selection in Faraday instability: Europhysics

Letters, **6**, 221 – 226.

Elboth, T., B. A. P. Reif Pettersson, and Ø. Andreassen, 2009, Flow and swell noise in marine seismic data: Geophysics, **74**, Q17 – Q25.

Faraday, M., 1831, On a peculiar class of acoustical figures; and on certain forms assumed by groups of particles upon vibrating elastic surfaces: Philososphical Transactions of the Royal Society of London, **121**, 299 – 340.

Haavik, K. E., and M. Landrø, 2016, Estimation of source signatures from air guns fired at various depths: A field test of the source scaling law: Geophysics, **81**, P13–P22.

Hatton, L., 2007, An empirical relationship between surface reflection coefficient and source array amplitude: http://www.leshatton.org/anelastic˙surface˙reflection˙coefficient.html, accessed 16 May 2017.

Hegna, S., and G. Parkes, 2011, The low frequency output of marine air-gun arrays: SEG Technical Program Expanded Abstracts 2011. Society of Exploration Geophysicists, 77–81.

Herring, C., 1941, Theory of the pulsations of the gas bubble produced by an underwater explosion: Report, Columbia Univ., Divison of National Defense Research.

Hovem, J. M., 2007, Marine acoustics, the physics of sound in underwater environments: Peninsula Publishing.

Hung, C. F., and J. J. Hwangfu, 2010, Experimental study of the behaviour of mini-charge underwater explosion bubbles near different boundaries: Journal of Fluid Mechanics, **651**, 55 – 80.

Ikelle, L. T., and L. Amundsen, 2005, Introduction to petroleum seismology: Society of Exploration Geophysicists.

Jensen, F. B., W. A. Kuperman, M. B. Porter, and H. Schmidt, 2011, Computational ocean

acoustics: Springer.

Jovanovich, D. B., R. D. Summer, and S. L. Akins-Easterlin, 1983, Ghosting and marine signature deconvolution: A prerequisite for detailed seismic interpretation: Geophysics, **48**, 1468 – 1485.

Krieger, J. R., and G. L. Chahine, 2005, Acoustic signals of underwater explosions near surfaces: Journal of Acoustical Society of America, **118**, 2961 – 2974.

Landrø, M., and L. Amundsen, 2014, Is it optimal to tow air guns shallow to enhance low frequencies?: Geophysics, **79**, A13–A18.

Landrø, M., and R. Sollie, 1992, Source signature determination by inversion: Geophysics, **57**, 1633 – 1640.

Lay, R. L., 1945, Repeated p-waves in seismic exploration of water covered areas: Geophysics, **10**, 467 – 471.

Loveridge, M. M., 1984, A study of the marine ghost: 46th Annual Meeting of the European Association of Exploration Geophysicists, London.

———, 1985, Marine seismic source signatures, directivity and the ghost: Thesis, University of Oxford.

Mayne, H. W., and R. G. Quay, 1971, Seismic signatures of large air guns: Geophysics, **36**, 1162 – 1173.

Meier, M. A., R. E. Duren, K. T. Lewallen, J. Otero, S. Heiney, and T. Murray, 2015, A marine dipole source for low frequency seismic acquisition: 85th Annual International Meeting, SEG, Expanded Abstracts, 176–180.

Nyborg, W. L., A. F. Scott, and F. D. Ayres, 1972, Tensile strength and surface tension of liquids, in American Institute of Physics Handbook, 3rd ed.: McGraw-Hill Book Company.

Oguz, H. N., and A. Prosperetti, 1990, Bubble oscillations in the vicinity of a nearly plane free surface: Journal of Acoustical Society of America, **87**, 2085 – 2092.

Parkes, G., and L. Hatton, 1986, The marine seismic source: Springer.

Périnet, N., D. Juric, and L. S. Tuckerman, 2009, Numerical simulation of Faraday waves: Journal of Fluid Mechanics, **635**, 1 – 26.

———, 2012, Alternating hexagonal and triped patterns in Faraday surface waves: Physical Review Letters, **109**, 164501–1 – 164501–5.

Rayleigh, O. M., 1917, On the pressure developed in a liquid during the collapse of spherical cavity: Philosophical Magazine Series 6, **34**, 94 – 98.

Robertsson, J. O. A., L. Amundsen, and Å. S. Pederson, 2016, Signal apparition for simultaneous source wavefield separation: Geophysical Journal International, **206**, 1301 – 1305.

Ronen, S., and S. Chelminski, 2018, A next generation seismic source with low frequency signal and low environmental impact: 80th Annual International Conference and Exhibition, EAGE, Extended Abstracts, TuE07.

Smith, J. G., 1999, Amplitude and phase effects of weather noise: 69th Annual International Meeting, SEG, Expanded Abstracts, 1485 – 1488.

Strandenes, S., and S. Vaage, 1992, Signatures from clustered airguns: First Break, **10**, 305 –312.

Temperley, H. N. V., and D. H. Trevena, 1979, Metastable effects associated with the reflection of a pressure pulse at the free surface of water: Journal of Applied Physics, **12**, 1887 – 1894.

ten Kroode, F., S. Bergler, C. Corsten, J. W. de Maag, F. Strijbos, and H. Tijhof, 2013, Broadband seismic data - the importance of low frequencies: Geophysics, **78**, WA3–

WA14.

Vaage, S., K. Haugland, and T. Utheim, 1983, Signatures from single airguns: Geophysical Prospecting, **21**, 87 – 97.

Wentzell, R. A., H. D. Scott, and R. P. Chapman, 1969, Cavitation due to shock pulses reflected from the sea surface: Journal of Acoustical Society of America, **46**, 789 – 794.

Weston, D. E., 1960, Underwater explosions as acoustic sources: Proceedings of the Physical Society, **76**, 233 – 249.

Willis, H., 1941, Underwater explosions, time interval between successive explosions: Report, British report.

LIST OF FIGURES

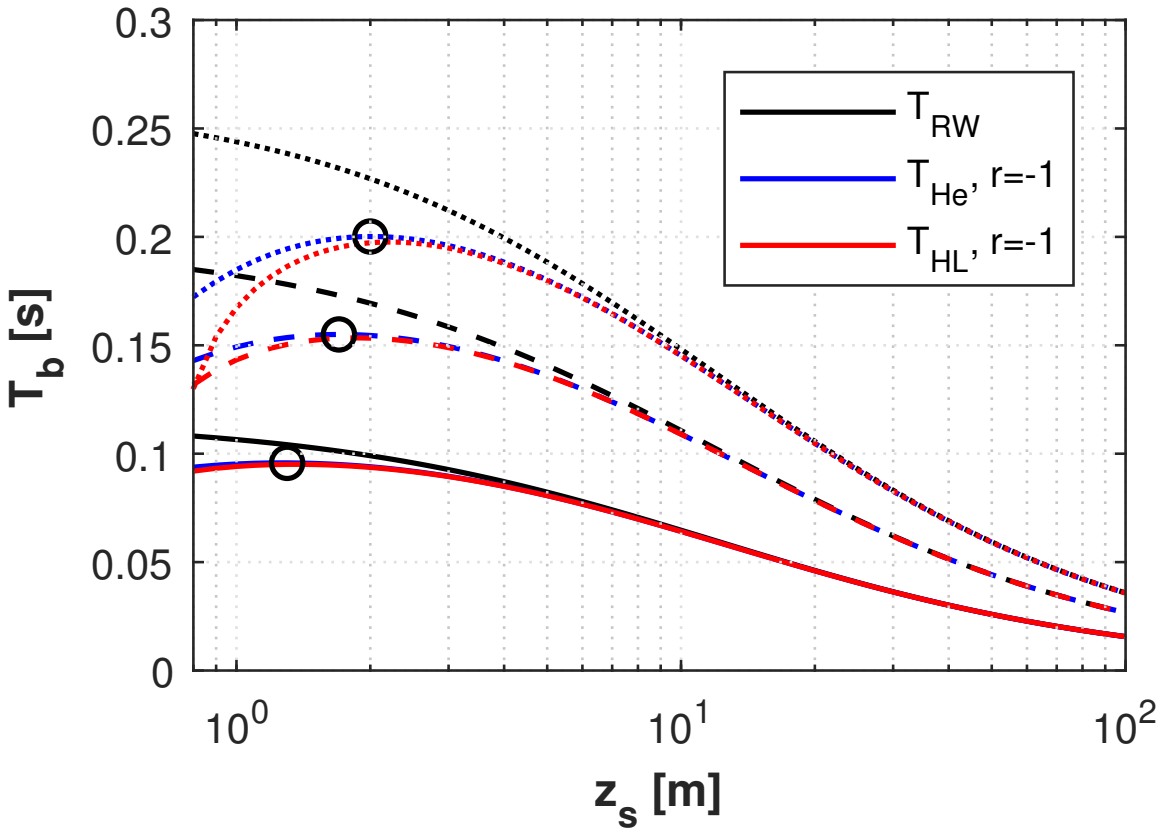

Figure 1: Change of bubble time period T_b in an infinite medium (T_{RW}) and close to a free surface (r = -1) for the different models, T_{He} and T_{HL}. T_b is modelled for different air gun sizes of 100 (solid), 500 (dashed) and 1200 (dotted) in^3 and a firing pressure of 137 bar. The circles indicate the maximum bubble period.

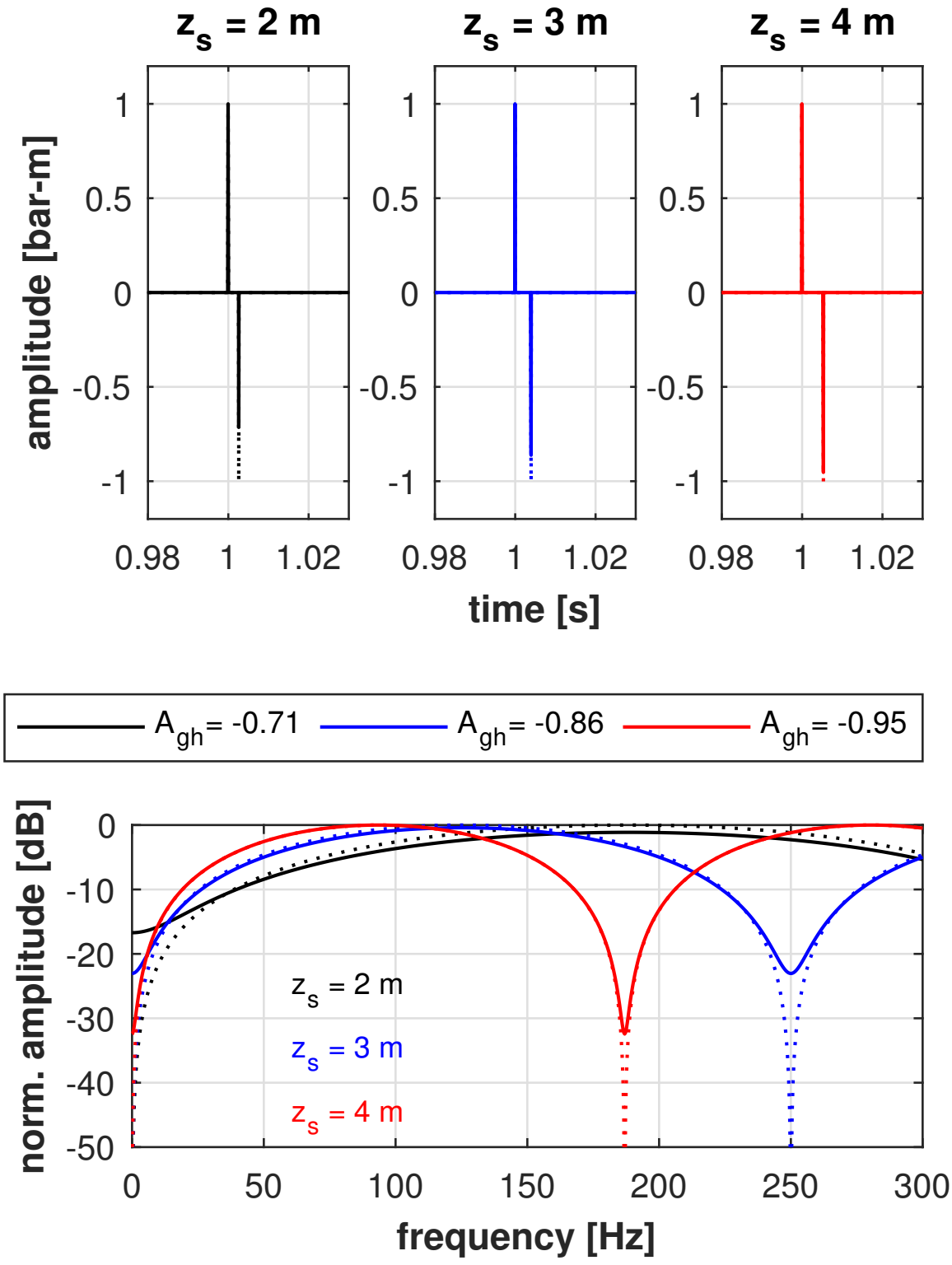

Figure 2: Spike functions and their ghost reflections from the sea surface (top) and the corresponding frequency spectra (bottom). Dashed lines indicate a prefect reflection at the surface. Solid lines indicate a reduced ghost reflection with amplitudes given as A_{gh}, computed from Equation 8.

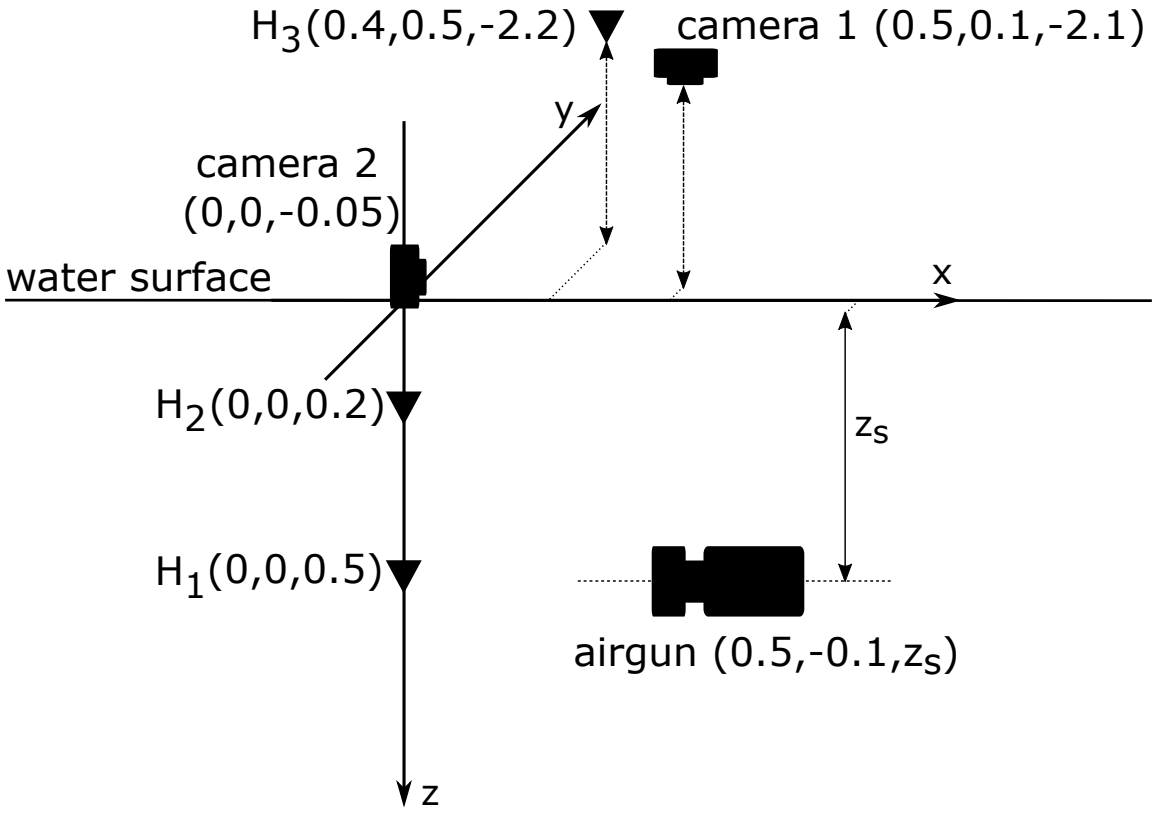

Figure 3: Sketch of experimental set up in the water tank. The hydrophones are indicated as H_1, H_2 and H_3 where the x-, y- and z-coordinates in meters are given in brackets. The water depth in the tank is 1.25 m and the width and length of the tank are 2.5 m and 6 m, respectively.

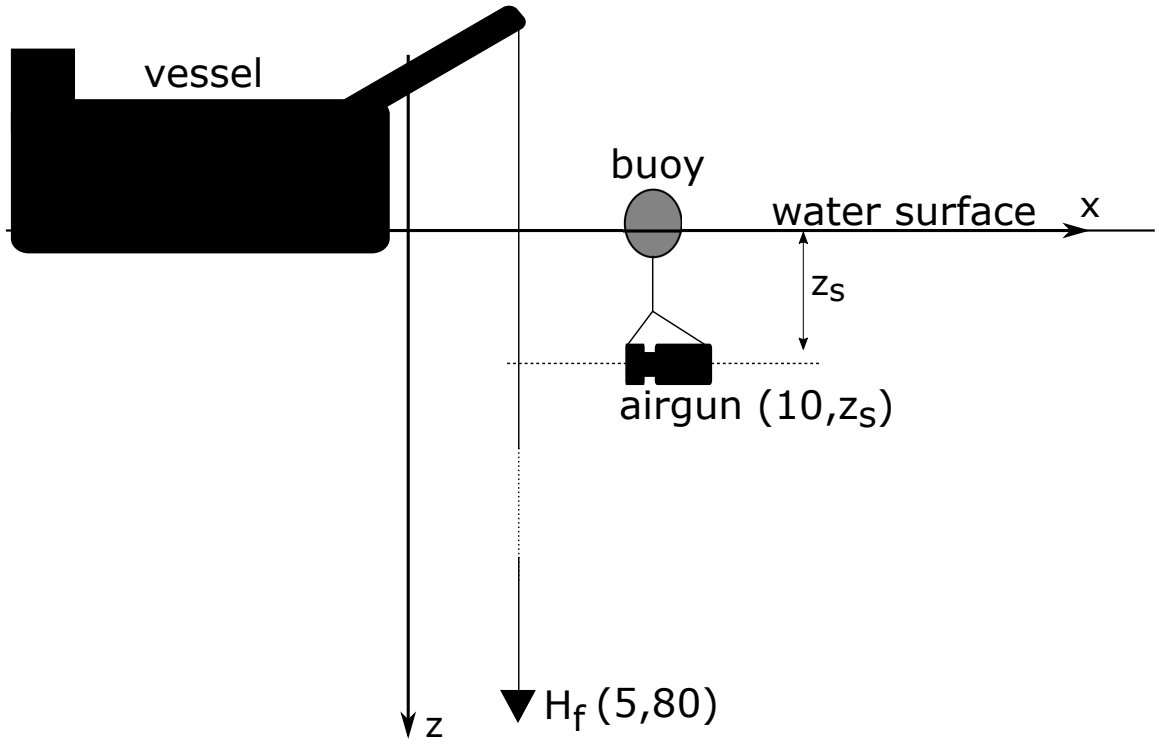

Figure 4: Sketch of experimental set up in the field. The hydrophone is indicated as H_f where the x- and z-coordinates in meters are given in brackets. The water depth in the fjord is around 390 m.

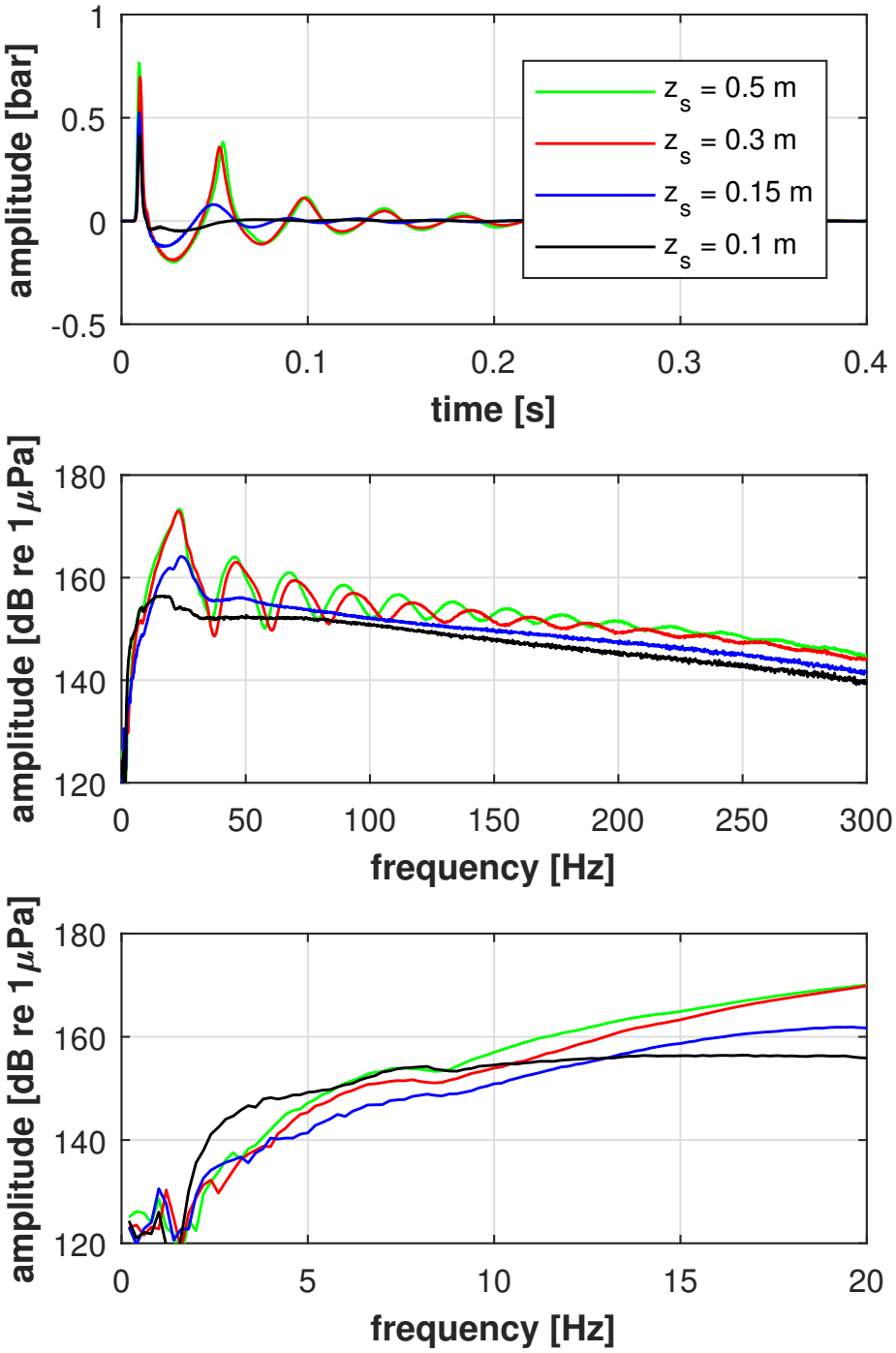

Figure 5: Measurements at H_1 of 12 in^3 air gun fired in water tank at different depths (top) and the corresponding frequency spectra (middle) and a zoom on the low frequency part (bottom). A 300 Hz low-pass filter is applied to the data.

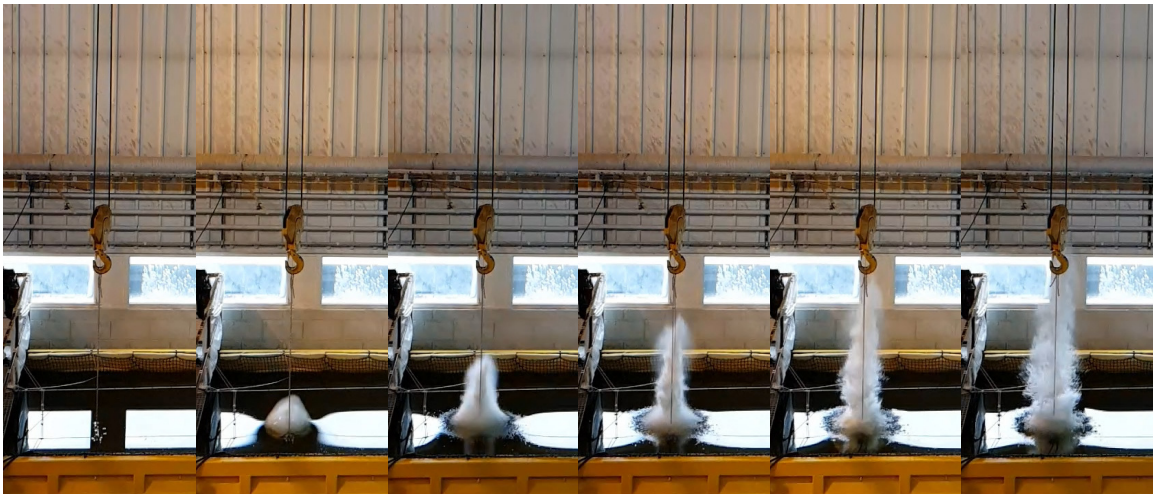

Figure 6: Photos of air gun fired at a depth of 0.15 m (taken by Stian Rørheim). The time between each photo is 13 ms.

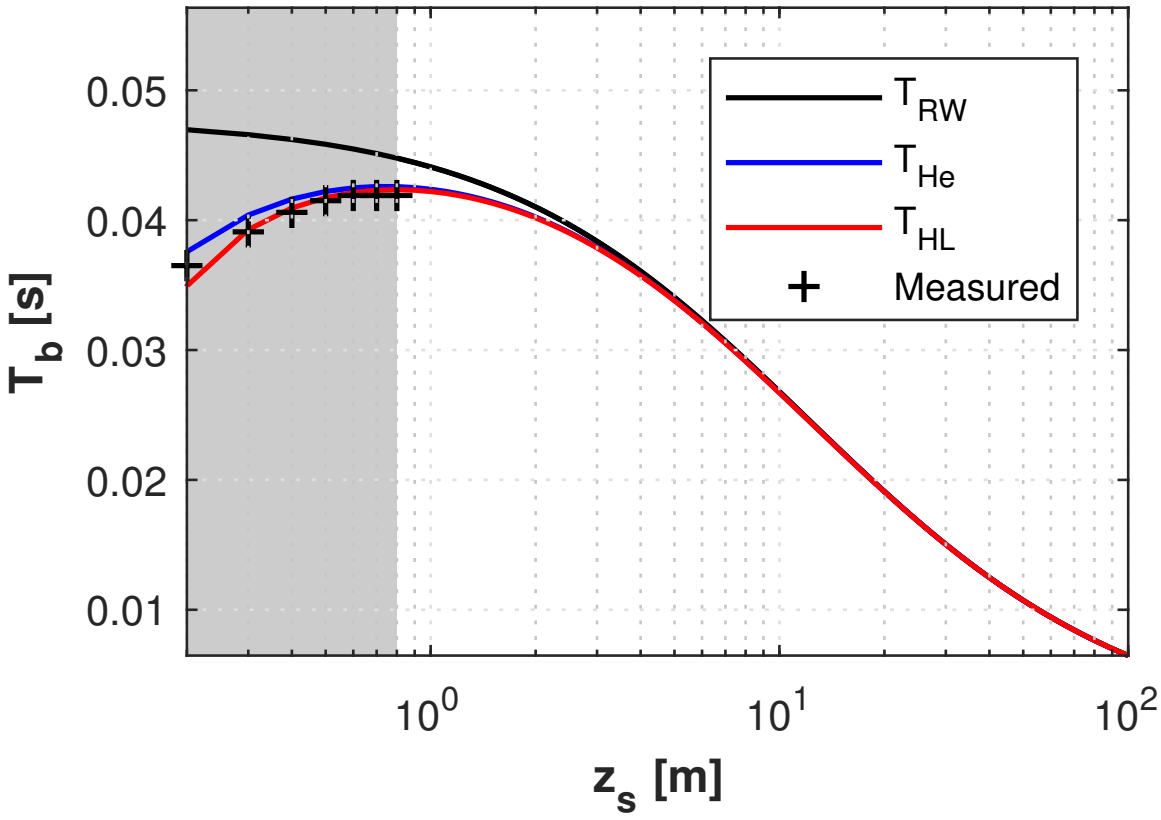

Figure 7: Measured bubble time period of 12 in^3 air gun for different depths fired in the water tank compared to theoretical curves from Rayleigh-Willis equation, Herring and Haavik (Eq. 1, 2, 3). The gray area indicates source depths which are smaller than four times the maximum bubble radius.

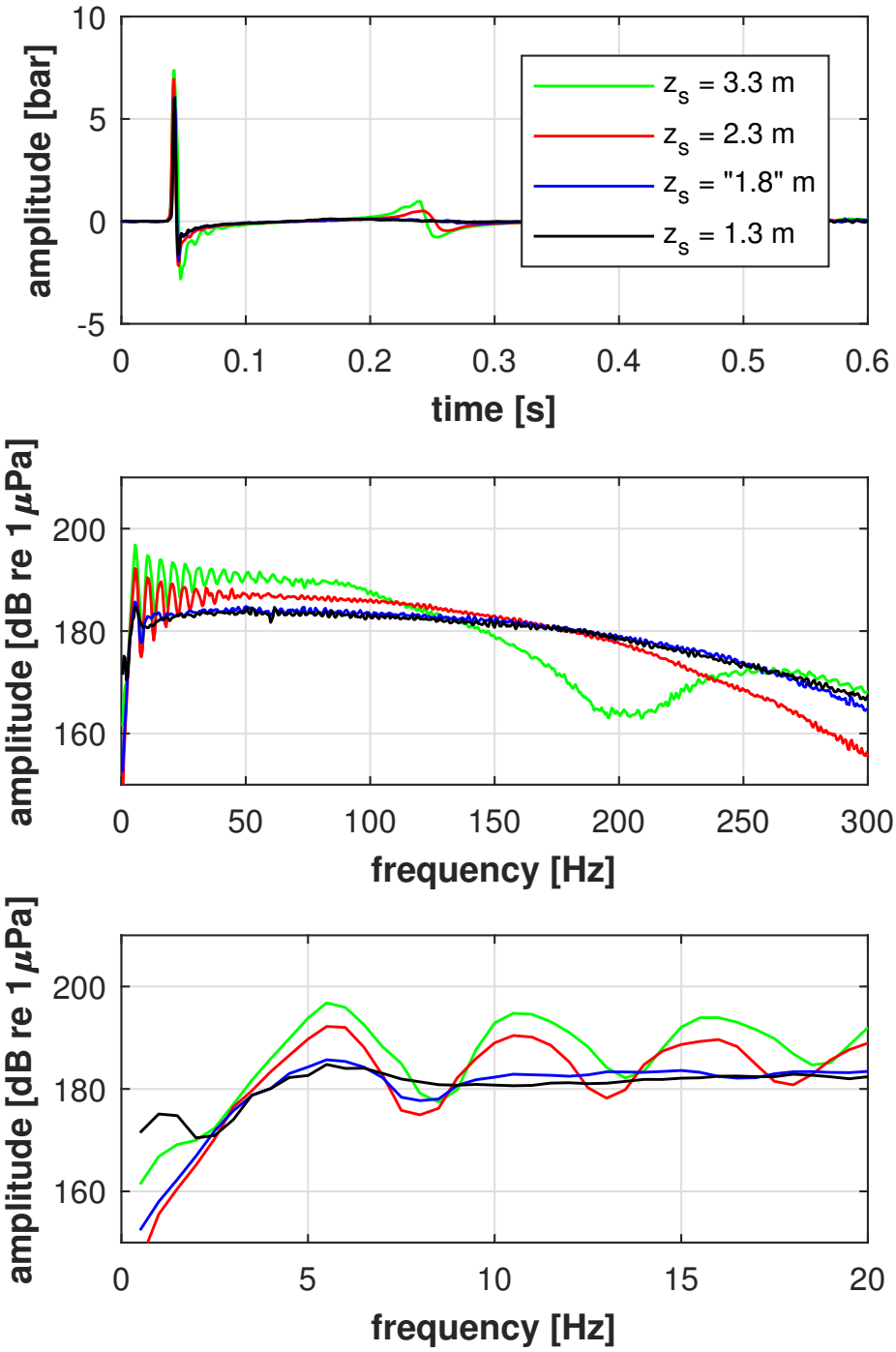

Figure 8: Measurements of 1200 in^3 air gun fired in the fjord at different depths (top) and the corresponding frequency spectra (middle) and a zoom on the low frequency part (bottom). A 300 Hz low-pass filter is applied to the data.

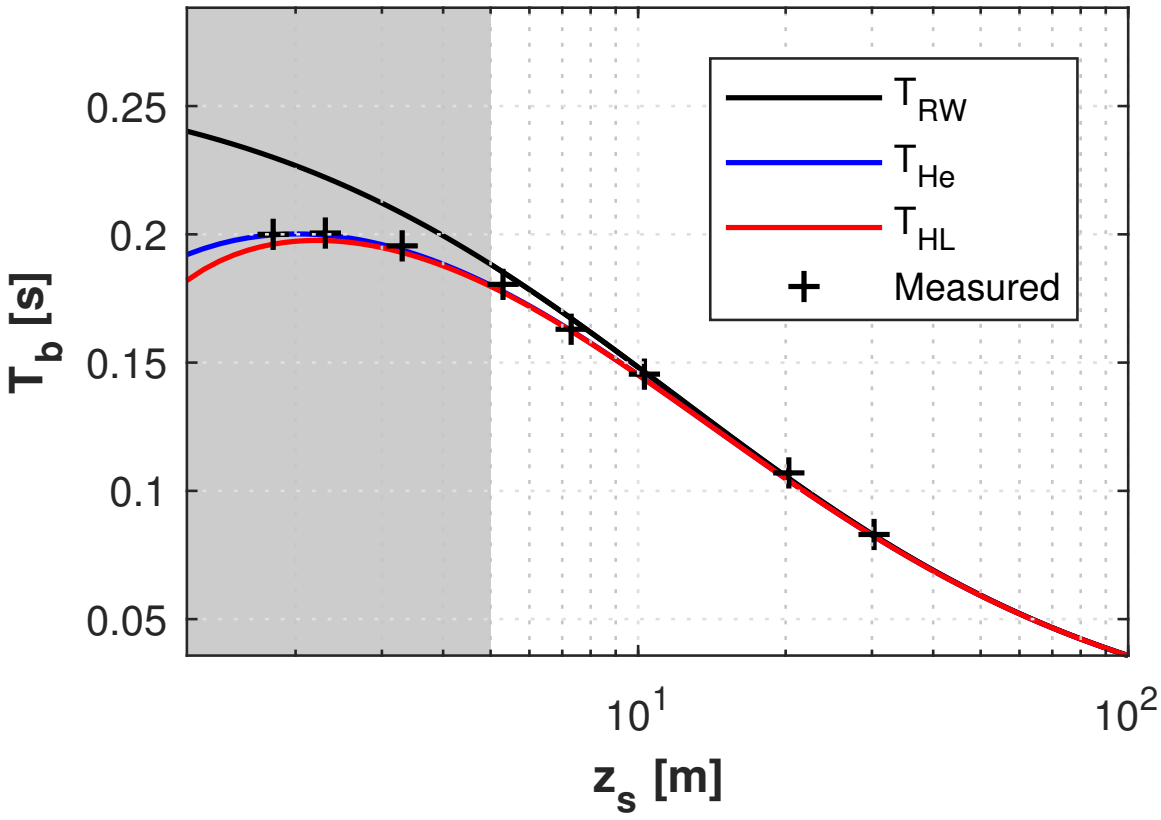

Figure 9: Measured bubble time period of 1200 in^3 air gun for different depths fired in the fjord compared to theoretical curves from Rayleigh-Willis equation, Herring and Haavik (Eq. 1, 2, 3). The gray area indicates source depths which are smaller than four times the maximum bubble radius.

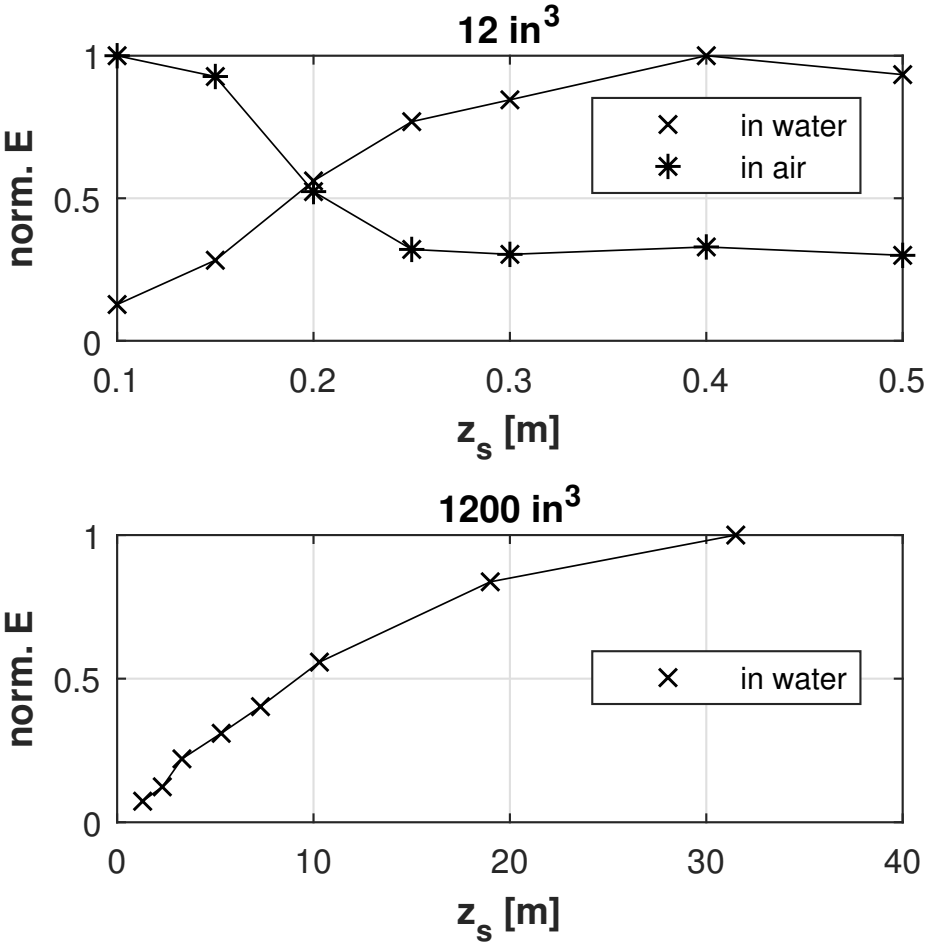

Figure 10: Estimated, normalized energy E using Equation 11 computed for different source depths for the tank experiments in air and water (top) and the field experiments (bottom).

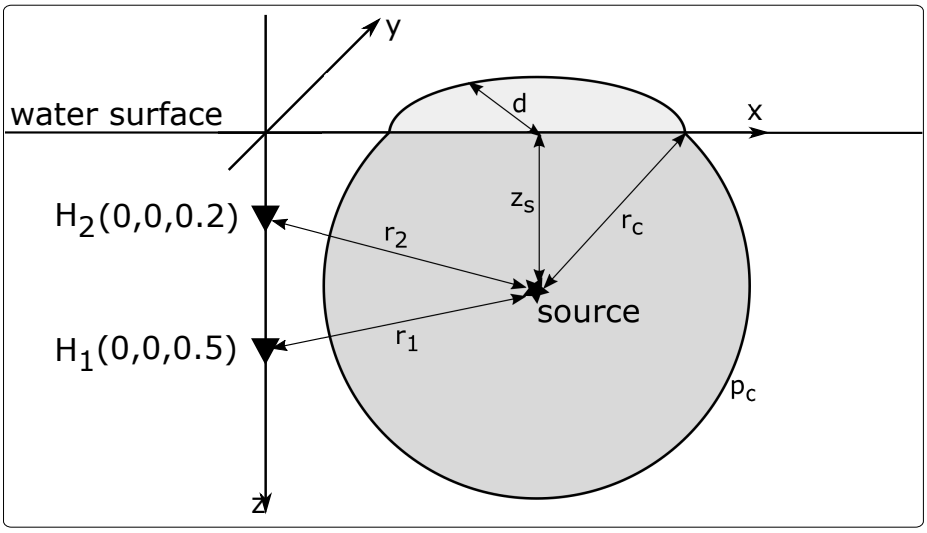

(a)

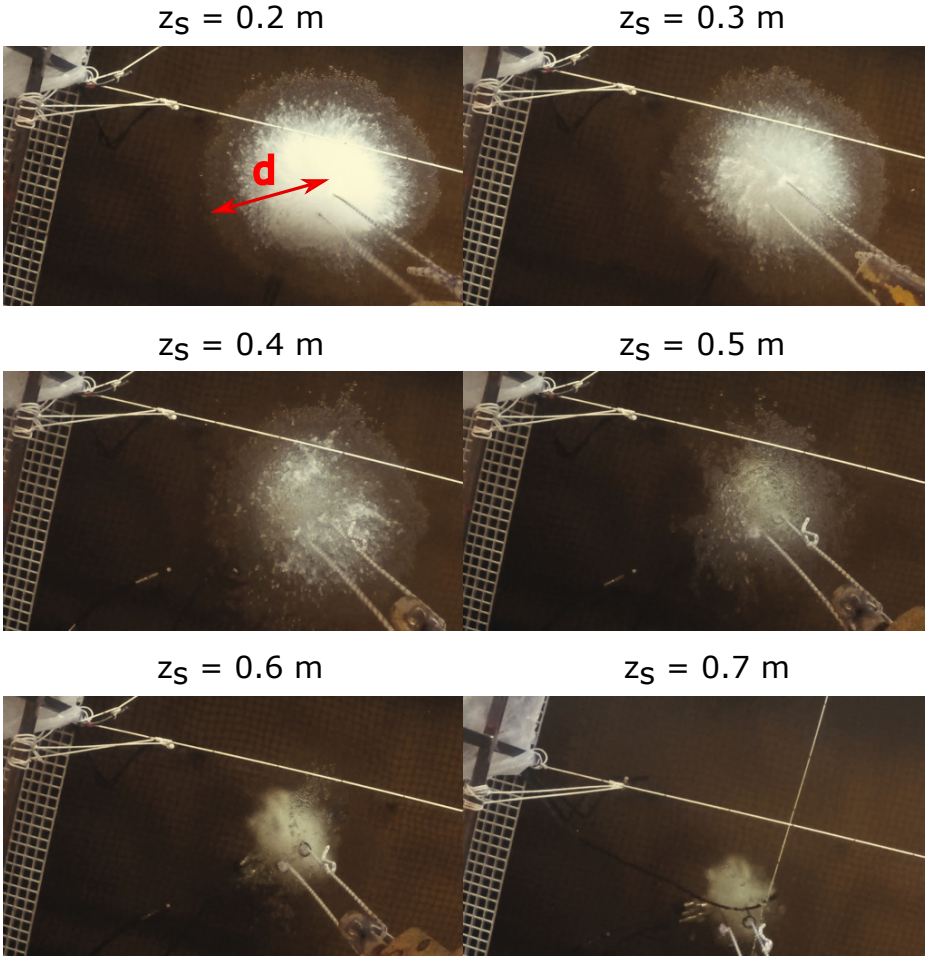

(b)

Figure 11: (a) Sketch illustrating the critical pressure p_c needed to disturb the surface area with the radius d. (b) Photos taken by camera 1 shown in Figure 3 of the air gun fired at different depths with a firing pressure of 80 bar. The photos are taken shortly after the main bubble radius was reached, at ca. 0.045 s (Figure 5).

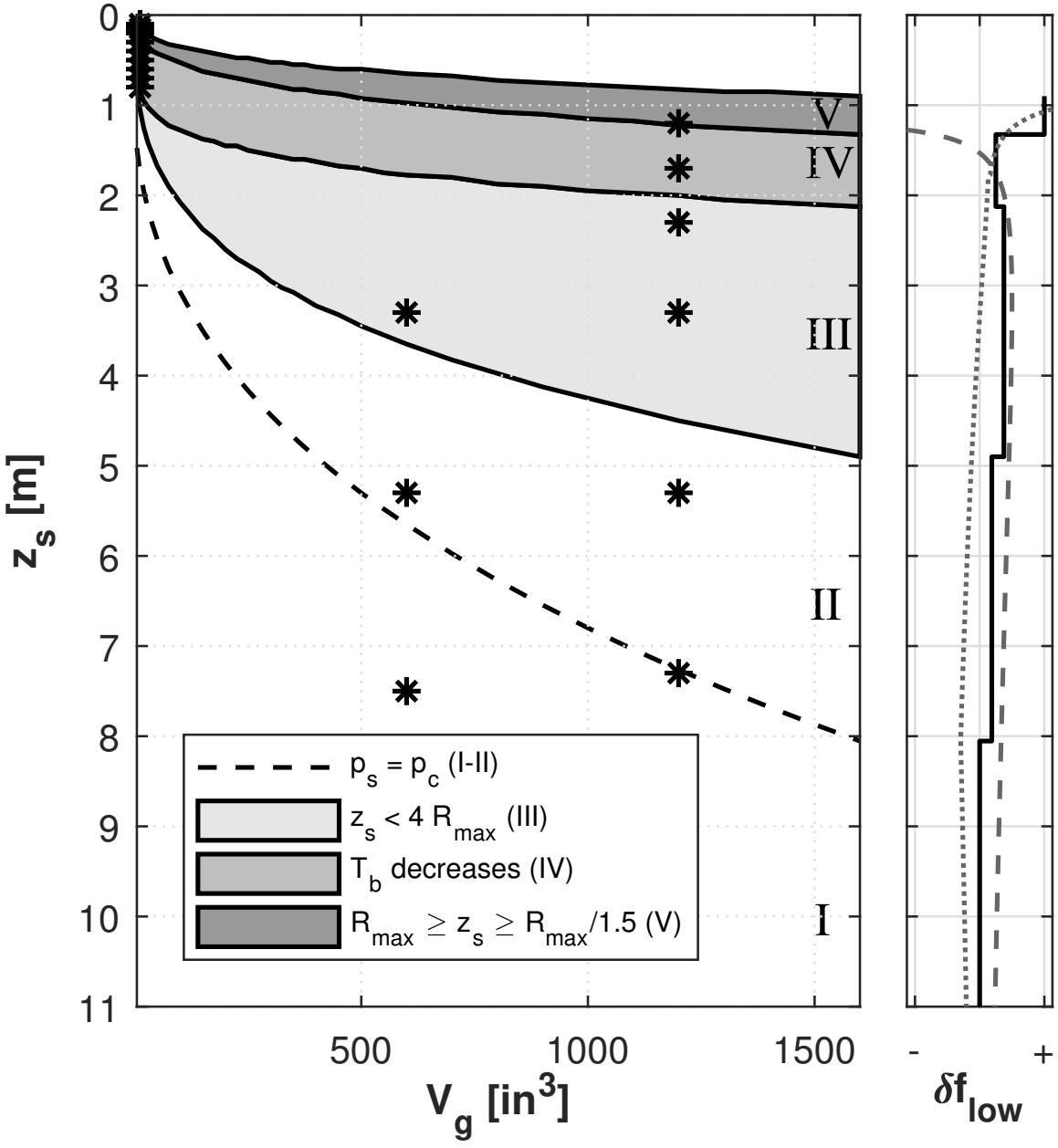

Figure 12: Left: Characteristic depths for different gun volumes V_g and a firing pressure of 137 bar as explained in point I to V. R_{max} is the maximum bubble radius, T_b the bubble time period, z_s the source depth, p_s the emitted acoustic pressure at the surface and p_c the critical pressure as indicated in Figure 11(a). Available measurements are indicated as asterisks. Right: relative variations of the low frequency content (< 5 Hz) with source depths, illustrated for $V_g = 1600$ in^3 (solid line) and the contributions from the bubble period (dashed line) and ghost effect (dotted line).